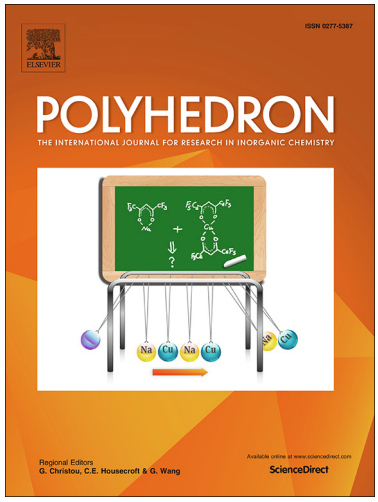

Fluorescent cyclic phosphoramide mustards and their cytotoxicity against cancer and cancer stem cells

Sudipta Bhattacharyya, Sourav Acharya, Suman Kr. Dey, Kavya Vipparthi, Sandeep Singh, Arindam Mukherjee

PII: S0277-5387(19)30384-5
DOI: https://doi.org/10.1016/j.poly.2019.05.046
Reference: POLY 13971

To appear in: *Polyhedron*

Received Date: 9 January 2019
Accepted Date: 24 May 2019

Please cite this article as: S. Bhattacharyya, S. Acharya, S.K. Dey, K. Vipparthi, S. Singh, A. Mukherjee, Fluorescent cyclic phosphoramide mustards and their cytotoxicity against cancer and cancer stem cells, *Polyhedron* (2019), doi: https://doi.org/10.1016/j.poly.2019.05.046

Fluorescent cyclic phosphoramide mustards and their cytotoxicity against cancer and cancer stem cells

Sudipta Bhattacharyya,[a] Sourav Acharya,[a] Suman Kr. Dey,[a] Kavya Vipparthi,[b] Sandeep Singh,[b] and Arindam Mukherjee*[a]

[a]Department of Chemical Sciences, Indian Institute of Science Education and Research Kolkata, Mohanpur- 741246, West Bengal, India

[b]National Institute of Biomedical Genomics, Kalyani-741251, West Bengal, India

Corresponding author e-mail: a.mukherjee@iiserkol.ac.in.

KEYWORDS. Phosphoramide mustard, x-ray structure, fluorescence, cytotoxicity, cancer stem cell

ABSTRACT

Two fluorescent cyclic phosphoramides, 1,3-dihydronaphtho[1,8-cd][1,2,6]phosphdiazine-2-oxide-(2-bis(2-chloroethyl)amide) (**1**) and 2,3-dihydro-2-oxo-1H-anthra[1,2-d][1,3,2]diazaphosphole-6,11-dione-2[N,N-bis(2-chloroethyl)]amide (**2**) were synthesized and characterized using standard analytical techniques. The single crystal X-ray diffraction studies of **1** showed that it crystallizes in triclinic space group *P*-1. The comparison of the bond distances and angles data of the single crystal structure of **1** with the theoretical value obtained from DFT calculations show that they are well commensurate with each other. ^{1}H and ^{31}P NMR studies reveal that **1** is more stable than **2** towards hydrolysis and formation of the active phosphoramide. **1** showed no dissociation in 48 h but 25% dissociation of **2** was observed using DMSO-phosphate buffer pH 7.4 (8:2 v/v). Compound **1** and **2** exhibit blue (λ_{em} = 375nm) and orange fluorescence (λ_{em} = 585 nm) respectively. However, the ligand of **2** daq exhibits red fluorescence (λ_{em} = 635 nm) in its free form. **1** and **2** showed cytotoxicity to cancer cells (MCF-7, A549, HepG2 and HeLa*WT*) and the toxicity enhanced *in vitro*, in presence of the cellular reducing agent ascorbic acid. The fluorescent imaging study of **2** showed that the intact compound enters organelles like mitochondria within 1h of treatment. The compound localizes in other organelles too and upon 10 h incubation red emissions from endoplasmic reticulum, mitochondria and lysozome suggests that the ligand daq dissociated from **2**. Compound **2** depolarises the mitochondria. Both **1** and **2** are efficient in killing the slow growing cancer stem cells (CSCs), known to cause cancer relapse. **1** and **2** also exhibit excellent anti cell migratory activity at IC_{10} dosage even after 48 h of removal of the compounds and causes cell death by apoptosis.

1. Introduction

Modifications of cancer chemotherapeutics are exercised to impart newer properties in an anticancer agent and generate molecules that would be more effective against cancer.[1-3] The tailoring through incorporation or alteration of appended moieties in existing anticancer agents had led to improvement in activity and brought new generation of drugs viz. the modification of cisplatin has led to oxaliplatin and carboplatin in clinic. The success of cyclophosphamide in clinic led to design of more compounds of this class by modification of the organic counter-part bound to the P(V). A list of such compounds is given in Table S1. Among them ifosfamide is in clinic and there are four more compounds (mafosfamide, evofosfamide, canfosfamide, glufosfamide) in clinical trials.

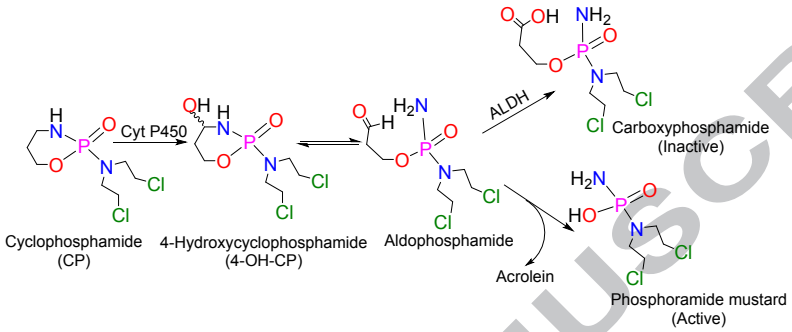

Scheme1. ALDH mediated deactivation of cyclophosphamide.

The parent cyclophosphamide has been more than 50 years in clinic and requires large dose to be administered due to high loss during metabolic activation.[4] In the liver cyclcophosphamide is hydroxylated by cytochrome P450 as described in Scheme 1. The hydroxylation leads to formation of aldehyde motif to generate aldophosphamide. This generated aldophosphamide loses the acrolein and becomes the active phosphoramide mustard. The generated acrolein is responsible for many side effects due to its excessive reactive nature and needs to be detoxified by additional drugs.[5] A significant amount of the active aldophoshamide species gets deactivated by the enzyme aldehyde dehydrogenase (ALDH) due to conversion to carboxyphosphamide.[6] Thus making cyclophosphamide less dose efficient.[7] Cardiac toxicity, gonadal failure are observed with high doses of cyclophosphamide and Hemorrhagic cystitis or bladder fibrosis can also be seen as a result of cyclophosphamide treatment.[8-11].

The inefficacy of cyclophosphamide due to its conversion to carboxyphosphamide by ALDH makes them inefficient against cancer stem cells (CSCs). Since certain isoenzymes of ALDH-superfamily are over expressed in CSCs and hence cyclophosphamide is not very efficient in killing CSCs.[12-14] CSCs, found in many solid tumors play a crucial role in metastases,[15, 16] resistance to chemotherapy/radiation,[17] and relapse.[18-20] Currently there is a dearth of CSC targeting drugs in clinic.[21] However, recent research have shown promises in this area. [20, 22-25] The impetus to this work was to use ligands that would generate traceable cyclophosphamides which cannot be deactivated by ALDH and thus would be active even against cancer stem cells.

We report here two cyclic phosphamides containing a tetrahedral P^V with N_3O bonding. Instead of the NO chelating aminopropanol in the clinically used cyclophosphamide or ifosfamide, we used N,N chelating 1,8-diaminonaphthalene (dan) to generate a 6-membered chelate (**1**) and 1,2-diaminoanthraquinone (daq) to generate a 5-membered chelate (**2**). Among the two compounds **1** was synthesized earlier but the crystal structure or the anticancer activities were not reported.[26-28] Our results show that both **1** and **2** exhibit excellent cytotoxicity profile with potential cell migration inhibitory activity at almost non-toxic dosage. Both the compounds are also active against CSCs and prohibited the formation of stem cell spheroid in A549 and HeLa*WT* cells at IC_{10} dose.

2. Experimental

2.1 Materials and methods

All chemicals and solvents were purchased from commercial sources. Solvents were distilled and dried prior to use, by standard procedure.[29] Phosphorus oxychloride and triethylamine used in the reactions were pre-distilled and dried before use. All the solvents are degassed and reactions were carried out under an atmosphere of dry nitrogen by following standard Schlenk techniques. MTT [(3-(4, 5-dimethylthiazol-2-yl)-2, 5-diphenyltetrazolium bromide)] (USB) and all kind of cell growth media, supplements were purchased from Gibco and used as received. All the solvents used for spectroscopic measurements are of spectroscopy grade and purchased from Merck, India. UV-Visible measurements were done using either Agilent Technologies Cary 300 Bio or Perkin Elmer Lambda 35 spectrophotometer. FT-IR spectra were recorded using Perkin-Elmer SPECTRUM RX I spectrometer in KBr pellets. NMR spectra were recorded using either JEOL ECS 400MHz or Bruker Avance III 500MHz spectrometer at ambient temperature and calibrated using residual undeuterated solvents as internal reference. Coupled and decoupled ^{31}P NMR data were recorded and reported relative to phosphorus signal of 85% H_3PO_4 (^{31}P, $\delta = 0.00$) as external standard. The chemical shifts (δ) are reported in parts per million (ppm). Elemental analyses were performed on a Perkin-Elmer CHN analyzer (Model 2400). Electro-spray ionization mass spectra were obtained from micromass Q-Tof micro^{TM} (Waters) in +ve mode electrospray ionization. The synthetic yields reported are of isolated analytically pure compounds.

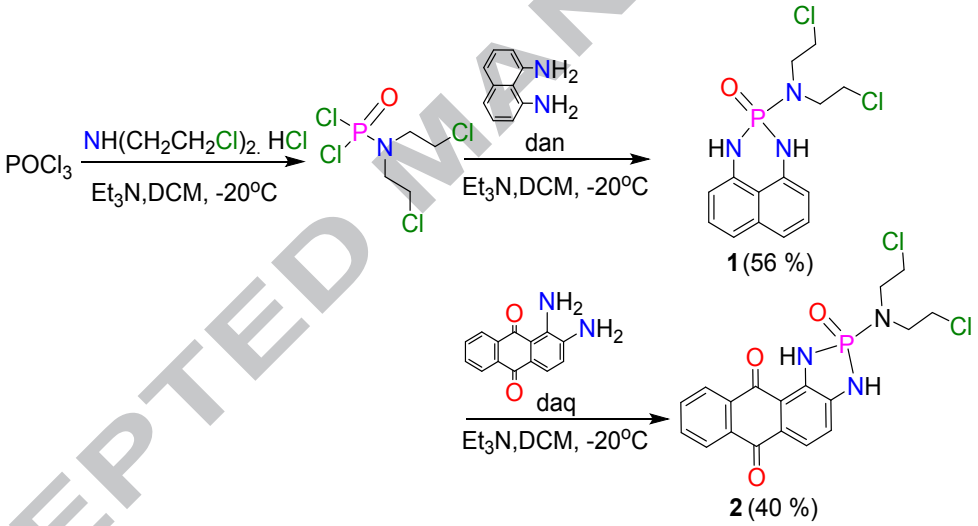

Scheme 2. Synthetic route for preparation of **1** and **2**.

2.2. Syntheses

Compound **1** was synthesized earlier using a three-step method. We used a two-step modified procedure which suitable for synthesis of both **1** and **2**. Hence we report the general procedure below.

2.2.1. Synthesis of N,N-bis(2-chloroethyl)phosphoramidicdichloride

The compound was synthesized following literature procedure in 1.0 mmol scale.[30] The entire crude product was used for next reaction step without further purification. The yield was assumed to be quantitative.

2.2.2. General synthetic procedure

A THF solution of N,N-bis(2-chloroethyl)phosphoramidic dichloride (1.0 mmol) was cooled in ice and slowly added to a mixture of diamine (1,8 diaminonapthalene for **1** and 1,2 diaminoanthraquinone

for **2**) (1.0 mmol) and triethylamine (2.0 mmol) in THF at –20 °C. Next the reaction mixture was left to stir for additional 2 h at the same temperature and ultimately brought to room temperature followed by stirring for another 10 h. The triethylamine hydrochloride thus produced was filtered and the filtrate was evaporated to dryness. The crude product was further purified by column chromatography on silica gel using mixture of solvent as eluent. Eluent composition for **1**, dichloromethane:methanol (9:1 v/v) and for **2**, dichloromethane:ethylacetate (7:3 v/v) (Scheme 2).

*2.2.2.1. 1,3-dihydronaphtho[1,8-cd][1,2,6]phosphdiazine-2-oxide-(2-bis(2-chloroethyl)amide) (**1**)*

Light orange-yellow crystals. Yield: 56%. m.p. 160°C; ^{1}H NMR (500 MHz, $CDCl_3$): δ = 3.51 (m, 4H, CH_2CH_2Cl), 3.67 (t, *J* = 6.12 Hz, 4H, CH_2CH_2Cl), 6.35 (s, 2H, NH), 6.57 (m, 2H, ArH), 7.22 (m, 4H, ArH); ^{13}C {^{1}H} NMR (125 MHz, $CDCl_3$): δ = 42.48 (CH_2CH_2Cl), 47.98 (CH_2CH_2Cl), 109.02 (ArC), 113.56 (ArC), 119.91 (ArC), 127.39 (ArC), 135.54 (ArC), 138.81 (ArC); ^{31}P {^{1}H} NMR (202 MHz, $CDCl_3$): δ = -0.016. HRMS Calcd. for ($C_{14}H_{17}Cl_2N_3OP$) [**1**+H]$^+$ (CH_3OH): m/z 344.0486, found, 344.0483; FT-IR. (KBr pellets, cm^{-1}): 3760 (w), 3425 (br), 3173 (s), 2955 (w), 2376 (s), 1600 (s), 1490 (m), 1395 (s), 1177 (s), 1072 (m), 985 (w), 906 (m), 813 (w), 770 (m), 757 (s); Elemental analysis Calcd. (%). for $C_{14}H_{16}Cl_2N_3OP$: C 48.86, H 4.69, N 12.21, found C 48.75, H 4.72, N 12.26; UV-vis (CH_3OH) λ (nm.) (ε/M^{-1}cm^{-1}): 233(33500), 321(11000), 335(10500), 350(9500). Quantum yield (MeOH): Φ = 0.40 (λ_{ex} = 330nm, Ref., Quinine sulphate).

*2.2.2.2. 2,3-dihydro-2-oxo-1H-anthra[1,2-d][1,3,2]diazaphosphole-6,11-dione-2[N,N-bis(2-chloroethyl)]amide (**2**)*

Reddish orange colour powder, Yield 40%; m.p. 255°C; ^{1}H NMR (500 MHz, DMSO-d_6): δ = 3.27 (m, 4H, CH_2CH_2Cl), 3.74 (m, 4H, CH_2CH_2Cl), 7.15 (d, 1H, *J* = 8 Hz, ArH), 7.72 (d, *J* = 7.6, 1H, ArH), 7.89 (m, 2H, ArH), 8.18 (m, 2H, ArH), 9.47 (t, *J* = 17.5 Hz, 2H, NH); ^{13}C {^{1}H} NMR (125 MHz, DMSO-d_6): δ = 42.22 (CH_2CH_2Cl), 47.36 (CH_2CH_2Cl), 113.21 (ArC), 120.51 (ArC), 123.75 (ArC), 126.23 (ArC), 126.61 (ArC), 133.10 (ArC), 133.41 (ArC), 133.58 (ArC), 133.92 (ArC), 134.22 (ArC), 139.05 (ArC); ^{31}P {^{1}H} NMR (202 MHz, DMSO-d_6): δ= 21.07. HRMS calcd. for ($C_{18}H_{17}Cl_2N_3O_3P$) [**2**+H]$^+$ (CH_3OH):m/z 424.0385, found 424.0381; FT-IR. (KBr pellets, cm-1): 3760 (w), 3350 (br), 3139 (br), 2370 (s), 1647 (s), 1592 (w), 1450 (s), 1286 (m), 1252 (m), 1214 (m), 1118 (s), 989 (m), 896 (m), 872 (m), 714 (m); Elemental analysis Calcd. (%). for $C_{18}H_{16}Cl_2N_3O_3P$: C 50.96, H 3.80, N 9.91, found C 51.41, H 3.92, N 10.01; UV-vis (CH_3OH) λ(nm.) (ε/M^{-1}cm^{-1}): 250(32500), 270(22000), 436(6200), 553(1500). Quantum yield (MeOH): Φ = 0.05 (λ_{ex} = 425nm, Ref., Coumarin 153).

Note: All the compounds after purification were dried and stored away from light and moisture under nitrogen environment in a refrigerator.

Caution! The compounds reported in this work are capable of alkylating DNA hence care should be exercised while handling them.

Methods

The details of X-ray crystallography, list of cyclophosphamide type compounds, NMR kinetics plot, MTT assay, FACS analysis for cell cycle and mitochondrial membrane potential change, Fluorescence microscopy imaging, ROS generation assay, DNA laddering assay for apoptosis, caspase activation, cellular localisation, wound healing assay and computational studies are provided in the supplementary data (Appendix A).

2.3. Cell lines and culture conditions

Human carcinoma cell lines used are of adherent nature and epithelial in morphology. MCF-7 (human breast carcinoma), A549 (human lung carcinoma), HeLa*WT* (Human cervical carcinoma) and HFF-1 (Human foreskin fibroblast) were kindly provided by Department of Biological Sciences, IISER-Kolkata, India. HepG2 (Human hepatocarcinoma) was procured from NCCS Pune, India. Cells were grown in T75 culture flasks as adherent monolayer in DMEM media supplemented with 10% heat-inactivated fetal bovine serum, 2mM L- glutamine, 1mM sodium pyruvate (Only for HepG2) and 100 units of penicillin, 100 µg mL^{-1} of streptomycin. Cultures were maintained in the logarithmic phase at 37 °C in a humidified atmosphere having 5% CO_2. For culture at hypoxia, only 1.5% of O_2 was used for cell growth and drug incubation. MCF-7 has been used as model cell line for all other biological assays other than cell viability screening.

2.4. Sub-cellular co-localisation of compound

Fluorescence microscopic technique was used to trace **2** inside cell. MCF-7 and HeLa*WT* were taken as cellular models to check versatility of compound localisation for this experiment. In all cases green fluorescence probes (known organelle targeting dye) has been used to determine the co-localisation with compound **2** (red fluorescence). MitoTracker Green™, LysoTracker green DND 26™ and ER-Tracker Green™ form Molecular Probes used to locate mitochondria, lysosome and endoplasmic reticulum respectively. Manufacturer protocol has been followed for treatment of dyes and our compounds. In all events, **2** (50µM) was treated for 10 h followed by washing with pre-warmed 1X PBS. Microscopic images for co-localisation were performed in Ziess Apotome microscope at 63X magnification. Exposure has been fixed in such a way that the background fluorescence could be minimised. In all cases threshold for co-localisation analysis was set as fixed by selecting dark pixels of image into consideration to minimise most of the possible artifacts. Image analysis was done using JaCoP co-localisation plug-in in ImageJ software.

2.5. Activity against cancer stem cells

2.5.1. Hoechst 33342 dye-efflux assay for Side-population (SP) analysis

Side-population (SP) analysis for CSC was performed following literature protocol in HeLa*WT* and A549 cells.[31, 32] A single cell suspension of 5×10^5 cells were seeded in a 35 mm tissue culture petri dish and cultured for 1 day in DMEM/F-12 media containing 10% FBS. Next the media was renewed and treated with IC_{50} concentration of **1**-**2**. Compound treatment was continued up to 48 h. After that media containing compounds were removed. Cells were harvested with Accutase (Invitrogen). 1×10^6 cells/mL were suspended in pre-warmed DMEM/F-12 medium containing 2% FBS and 15mM HEPES. Cells were incubated with 4 µg/ml of Hoechst 33342 dye (Invitrogen) for 90 minutes at 37°C in presence or absence of 1 µM of a selective inhibitor of ABCG2-transporter, Fumitremorgin C (FMC) (Sigma) During incubation cells were mixed every 15 min by tapping. Next, cells were centrifuged at 400 rcf for 3 min and pellets thus obtained were re-suspended in cold Hanks Balance Salt Solution (HBSS) supplemented with 0.5% FBS. Propidium Iodide (PI) was added to each tube to discriminate live and dead cell population. The Hoechst dye was excited with a near UV laser (375 nm) and respective double emission was measured at 515 nm (blue emission) and 608 nm (red emission) filter in BD Accuri–SORP flow cytometer. Data was analysed using BD AccuriC6 software (BD). Experiments were done in triplicate.

2.5.2. Sphere forming assay

HeLa*WT* and A549 cells (500 cells/well) were plated in an ultra-low attachment 96 well plate. Cells are grown in 100 µL serum free media (DMEM/F-12) supplemented with 1X antibiotic-antimycotic solution (Gibco), hydrocortisone (0.4 µg/mL), 1X N-2 supplement (5 µg/mL), epidermal growth factor (20 ng/mL), basic fibroblast growth factor (20 ng/mL). In such condition only self-renewing, cancer stem cells are able to grow and form spheres.[33, 34] Cells were treated with compounds from the beginning of experiment dissolving the same in the growth media. On every alternate day 20 µL of growth supplement was added in each well. On 5th (for HeLa*WT*) and 7th day (for A549) spheres of size above 60 microns were counted from the respective images captured with inverted microscope [Olympus CKX41].

3. Results and Discussion

3.1. Synthesis and characterization

We synthesized two cyclic phosphoramides **1** and **2**, where the ligands are 1,8-diaminonapthalene (dan) & 1,2-diaminoanthraquinone (daq) respectively (Scheme 2). Compound **1** was synthesized earlier but the crystal structure or the cytotoxicity against cancer cells are not reported.[26, 27] We used a modified synthetic procedure, involving one less step, which was suitable for synthesis of both **1** and **2**. The purification of **1** or **2** involved flash column chromatography using 100-200 mesh silica gel since there were multiple products formed in minor quantities which could not be separated otherwise. The column chromatography was done as quickly as possible to avoid any possible degradation of products in the column. **1** provides a six membered ring upon N,N chelation with the P^V. N,N chelation by the daq in **2** gave a 5-membered ring. Both the ligands have N,N chelation but dan forms a six membered chelate with the P^V in **1** (Fig. 1) whereas daq forms a five membered chelate with the P^V in **2**. The six membered chelate forming **1** showed tighter binding to the P^V then the five membered chelate forming **2**. The presence of the anthraquinone oxygens also dragged electron density from the donor nitrogens and hence compound **2** showed less stability than **1**.

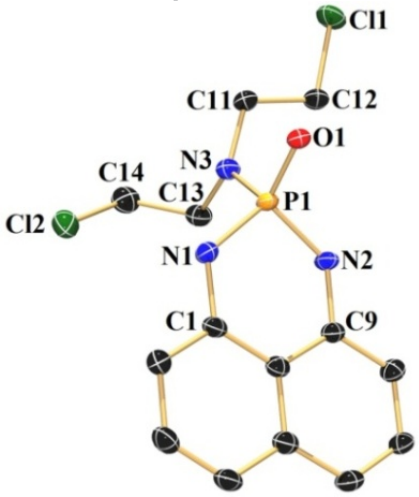

Fig. 1. ORTEP diagram of **1** with thermal ellipsoids at 50% probability level. Hydrogen atoms are omitted for clarity.

The difference in the stability of the two compounds also affected their cytotoxic activity. The ^{31}P NMR showed signals at -0.016 (t) and 21.07 (m) ppm for **1** and **2** respectively. Difference in the multiplicity of the ^{31}P signal in **1** and **2** demonstrated that the chelated nitrogen atoms are equivalent in **1** but non-equivalent in **2** (Scheme 2). The non-equivalence may be assigned to the difference in proximity of the anthraquinone group to the two coordinating nitrogens. Compound **1** and **2** both exhibit N_3O coordination

(Scheme 2) and were duly characterized for purity using various analytical methods. **1** crystallized in Triclinic space group *P*-1 (Fig. 1). It must be noted that single crystal structures of phosphoramide mustards are scarce.[35-37] In the asymmetric unit of **1**, all the molecules are not equivalent. There are two molecules in one asymmetric unit due to changes in the orientation of the chloroethyl amine group (the mustard motif) attached with the P centre. Selected crystallographic parameters are summarized in Table S2 and S3.

The average P-N and P=O bond distance is **1** was found to be 1.644 (2) and 1.491(1) Å respectively. The O-P-N angle were in the range of ca. 106 -117° and the N-P-N angles ranged between 101-110°. Single crystals of compound **2** were not suitable for X-ray diffraction. Hence, the computational studies were performed for obtaining the optimized structure to get a better insight of structural orientation and energy of **2**. Calculations were performed at DFT level of theory with BVP86 function and 6-31G(d,p) basis set for both **1** and **2** (Fig. S1 and Table 2). The comparison of the bond distances and angles data of the single crystal structure of **1**with the theoretical value obtained from DFT calculations suggest good agreement (Table 2). Since, the bond distance and angle data of **2** were obtained using the same method hence they provide a good representation of few essential structural parameters in absence fo the crystal structure of **2**.

Table 2.

A comparison of selected bond angle (°) and bond distances (Å) of **1** and **2** from energy optimised structure [a] and crystal structure.[b]

Experimental		Theoretical		Theoretical	
		1		**2**	
P(2)-N(4)	1.640(2)	P(13)-N(11)	1.689	P(19)-N(17)	1.717
P(2)-N(5)	1.631(2)	P(13)-N(12)	1.688	P(19)-N(18)	1.700
P(2)-N(6)	1.659(2)	P(13)-N(15)	1.708	P(19)-N(21)	1.674
P(2)-O(2)	1.492(2)	P(13)-O(14)	1.505	P(19)-O(20)	1.485
Cl(3)-C(26)	1.801(3)	Cl(21)-C(26)	1.830	Cl(24)-C(23)	1.813
Cl(4)-C(28)	1.800(3)	Cl(20)-C(18)	1.830	Cl(27)-C(26)	1.814
N(4)-C(15)	1.395(4)	N(11)-C(6)	1.411	N(17)-C(2)	1.395
N(5)-C(23)	1.404(4)	N(12)-C(10)	1.411	N(18)-C(1)	1.385
Experimental		Theoretical		Theoretical	
		1		**2**	
O(2)-P(2)-N(6)	106.49(11)	O(14)-P(13)-N(15)	117.38	O(20)-P(19)-N(21)	110.25
O(2)-P(2)-N(5)	116.77(11)	O(14)-P(13)-N(12)	114.60	O(20)-P(19)-N(18)	120.81
O(2)-P(2)-N(4)	114.61(11)	O(14)-P(13)-N(11)	114.03	O(20)-P(19)-N(17)	117.96
N(5)-P(2)-N(4)	101.18(11)	N(12)-P(13)-N(11)	99.49	N(18)-P(19)-N(17)	89.50
N(5)-P(2)-N(6)	107.55(12)	N(12)-P(13)-N(15)	104.55	N(18)-P(19)-N(21)	107.48
N(4)-P(2)-N(6)	110.00(12)	N(11)-P(13)-N(15)	104.75	N(17)-P(19)-N(21)	108.86

[a] Structures were optimised using BVP86/6-31G(d,p) in methanol as solvent. [b] Single crystal XRD data of **1**.

Calculations revealed that the energy gap between HOMO and LUMO of **1** is greater (HOMO= -4.74 eV, LUMO= -1.81 eV, $\Delta E_{HOMO-LUMO}$ = -2.93 eV) than **2** (HOMO= -5.42 eV, LUMO= -3.56 eV, $\Delta E_{HOMO-LUMO}$ = -1.86 eV). From TD-DFT calculations it was confirmed that in both cases major contributor of electronic transitions was HOMO→LUMO (Fig. S2). The predicted electronic transitions as per the TD-DFT calculations showed good agreement with most of the observed electronic transitions as depicted in Table 3.

The designing of **1** and **2** involved use of fluorescent ligands to enable visualization upon their entry in cell. The fluorescence of **1** showed emission in the blue region (λ_{ex} = 350 nm, λ_{em}= 375nm) (Fig. S3A and S5A). In case of **2**, the excitation at the absorption maxima of 436 nm produced maximum fluorescence intensity at λ_{em}= 585 nm (Fig. S3B & 5B). The ligand daq is known and observed to exhibit red fluorescence in solution (λ_{ex} = 547 nm, λ_{em} = 635 nm) (Fig. S4).[38, 39] A significant blue shift among the absorption spectra of daq and **2** can be explained in terms of the extended conjugation of the aromatic electron cloud with the free lone pairs of amine which is interrupted in case of **2**. P-N bond formation drags the make the electron density towards the P(V) leaving one of the aromatic rings apart from it as seen in both HOMO and LUMO of **2**. This drift in electron density in **2**, over the well distributed π-electron density in daq made the HOMO-LUMO energy gap more leading to electronic transition of higher energy. This phenomenon led to a change in the excitation wavelength for the free ligand (λ_{ex} = 547 nm) and **2** (λ_{ex} =495 nm). It also provided a significant blue shift in the emission spectrum of **2** (λ_{em} = 585 nm) compared to the free daq (λ_{em} = 635 nm). This particular shift became important to detect the free ligand from **2** as discussed later in the fluorescence microscopy section.

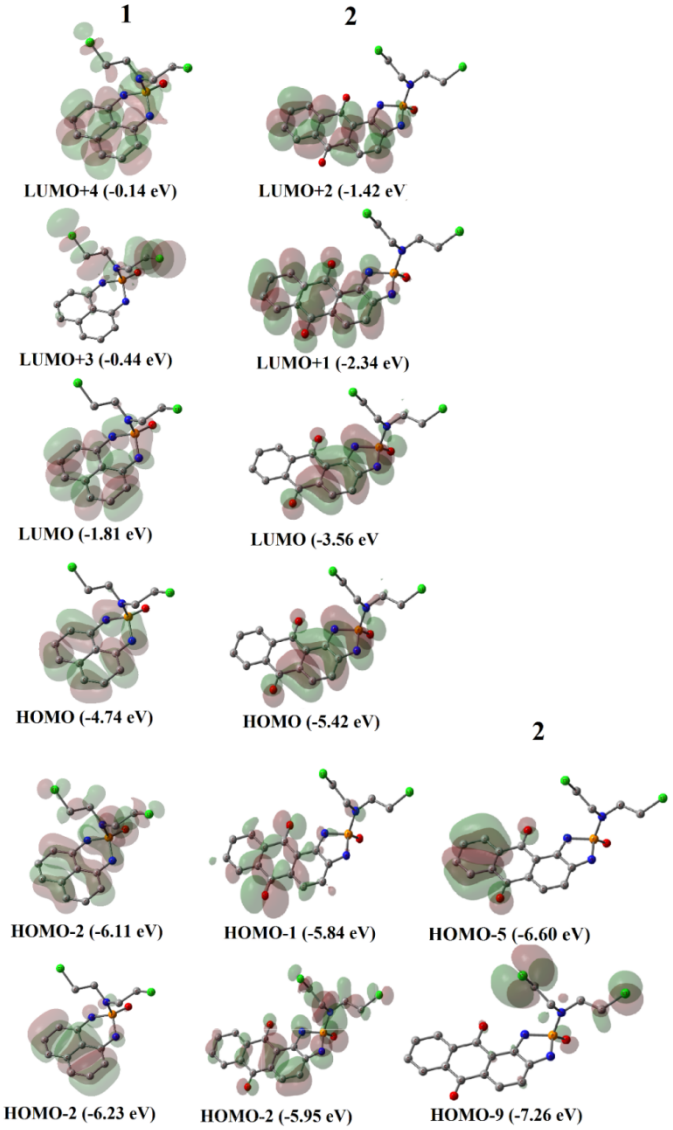

Fig. 2 Selected molecular orbital diagram involved in major electronic transitions of **1** & **2**, calculated from DFT calculation at level of B3LYP/6-31G(d) in methanol as solvent (CPCM model).

Table 3

Selected electronic transition data obtained by TD-SCF DFT method using B3LYP/6-31G (d,p) considering methanol as solvent in CPCM model.

Compound	λ_{abs}	Energy(cm^{-1})	Osc. strength	Major MO contributions [a]
1	321.9	31057.4	0.2106	HOMO→LUMO (97%)
	230.5	43386.5	0.2123	H-2→LUMO (43%), HOMO→L+3
	218.5	45764.2	0.4102	H-3→LUMO (24%), H-2→LUMO
2	442.3	22608.7	0.2136	HOMO→LUMO (98%)
	288.5	34664.3	0.1483	H-5→LUMO (89%)
	262.6	38085.8	0.2826	H-2→L+1 (11%), H-1→L+1 (70%),
	248.1	40303.0	0.2458	H-9→LUMO (25%), H-1→L+1 (10%),
	246.3	40596.6	0.1188	H-9→LUMO (60%), HOMO→L+2

[a] Orbital contributions has been determined using GaussSum 2.2 software package from Gaussian output file.

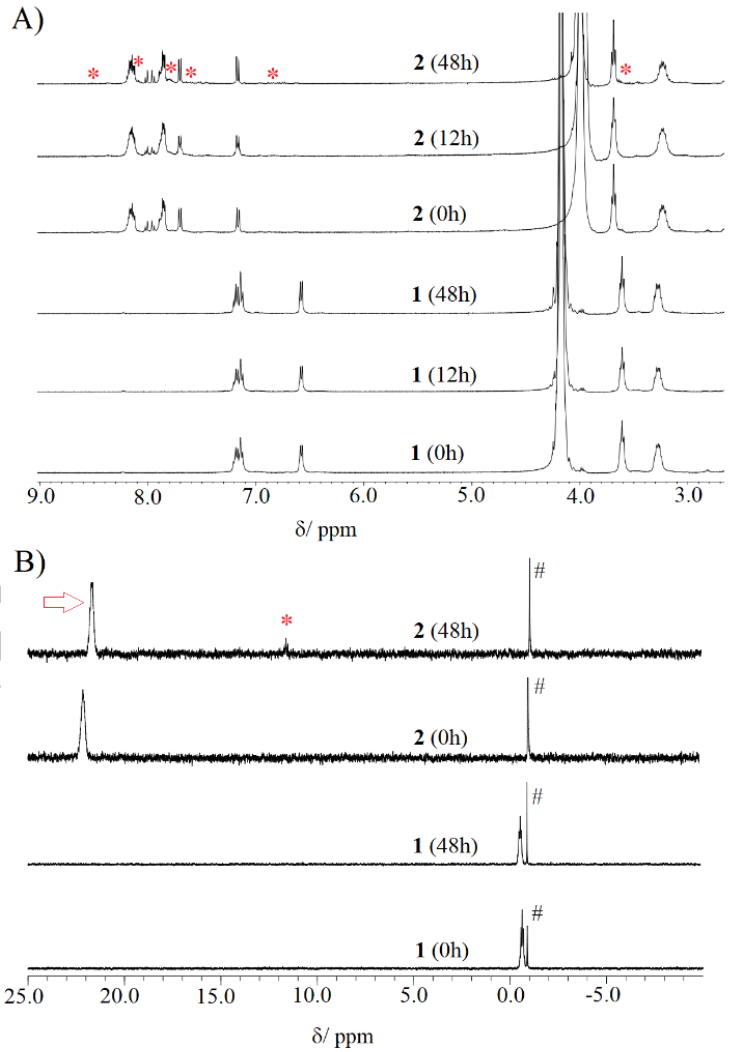

Fig. 3. Solution stability of **1** and **2** in 8:2 (v/v) DMSO-d_6/D_2O containing 4mM NaCl (pD = 7.4) up to 48 h. A) ^1H NMR, B) ^{31}P NMR spectral traces of corresponding compounds shown for comparison. Ligand release is shown by (*) and (#) signifies inorganic phosphate.

3.2. Solution stability studies

The stability of **1** and **2** in DMSO-phosphate buffer (8:2 v/v) was probed by ^{1}H NMR at 25°C in pH 7.4. The compounds do not show any change within 10 h (Fig. S6, S7). Spectral changes in $–NCH_2CH_2Cl$ protons were calculated to determine stability. The result showed that, **1** is more stable in 8:2 (v/v) DMSO-d_6: PBS (pD = 7.4) in comparison to **2** (Fig. 3A & S6). However, even for **2** there was no dissociation in presence of 110mM NaCl after 48 h (Fig. S7). Overall, the^{1}H NMR studies indicate that **1** is more stable than **2**. The ^{31}P NMR studies also supported higher stability of **1** (Fig. 3B). We also studied the influence of H_2O vs. D_2O for **2** by studying the hydrolysis in DMSO-d_6: Phosphate buffer in H_2O (8:2 v/v) containing 4mM NaCl, since hydrolysis rates are more in H_2O than D_2O (Fig. S8). Compound **2** was found to have faster decay in the aforementioned H_2O containing medium. This may be attributed to the relatively less stable 5-membered N,N chelated P^V in **2**. Compound **2** showed ca. 20% hydrolysis after 48 h in 8:2 (v/v) DMSO-d_6: PBS (pH = 7.4) containing 4mM NaCl (Fig. S8). The above data suggests that the hydrolyzed species may be in equilibrium with the native compound. In case of **2,** after 6 h a small but distinguishable shift of ca. 0.3 ppm was visible in the native ^{31}P signal which may be due to interaction of the DMSO with the hydrogen of –NH, which is known to occur.[40] In ^{31}P NMR studies of **2**, after 36 h, a new peak starts to appear ca. 11 ppm suggesting the formation of phosphoramic mustard (Fig. 3B & Fig. S9). The formation of the phosphoramic mustard should, in principle, be promoted by the presence of a base. We studied the influence in **2** and found that the addition of catalytic amount of NaOH indeed accelerated the formation of the phosphoramic mustard and the formation started to be visible just after 6 h and became prominent by 12 h, instead of 36 h (Fig. S10 and Table S5).

3.3. Cytotoxicity studies

The *in vitro* cytotoxicity of **1** and **2** were probed against a selected panel of human cell lines, viz., breast adenocarcinoma (MCF-7), human lung adenocarcinoma (A549), human hepatocellular carcinoma (HepG2) and primary human foreskin fibroblast (HFF-1). The potential of **1** & **2** in both normoxia and hypoxia were probed and **2** was found to be the most effective one. None of the free ligand (dan or daq) showed any toxicity up to 180 μM (Table S6). The observed IC_{50} of **1**, ranges from 68.6(1)-109.8(1) μM in the probed cancer cell lines. **1** is most active against HepG2 (IC_{50} = 68.59(5)μM) and is comparatively less toxic (IC_{50} = 125.4(3) μM) against the primary cell line HFF-1 (Table 1). In spite of lower cytotoxicity the higher selectivity towards cancer exhibited by **1** is an encouraging profile in an anticancer agent. Both the compounds showed enhanced activity in presence of the ascorbic acid (vitamin C). Ascorbic acid is known to influence the cytotoxicity including that of cyclophosphamide by disrupting the cellular redox balance.[41-45] Ascorbic acid is transported into the cells by several receptors including GLUT receptors [46, 47]. In cellular environment the formation of ROS assisted by H_2A would lead to generation of dehydroascorbic acid which in turn may oxidize cellular GSH to GSSG. Hence, in presence of more ascorbate, there will be more conversion of GSH to GSSG and enhancement of ROS. Thus, the cellular GSH would be deactivated and cannot bind to the compounds preventing it from deactivating the compounds leading to higher toxicity of **1** and **2** (Table 4).

3.4. Cellular imaging studies

The fluorescence of **1** was blue, the excitation needed UV laser and in addition could be interfered by back ground cellular fluorescence. Hence, it was not probed for fluorescence imaging. In contrast, the orange fluorescence of **2** or the red fluorescence of free daq enabled the visualisation of the targeting organelles (Fig. S11 & S13**)**. In the recent past it was shown that daq resides in the cytosol.[39] The results of the fluorescence microscopy suggested that **2** localizes in various cytosolic organelles. To further confirm if dissociation occurs after reaching the organelles, a confocal microscopy study was performed on suggestion by the reviewer, after 1 h of treatment with **2**. The images showed mostly intact **2** localizes in mitochondria in the breast cancer cells when we used mitotracker green to study the colocalization (Fig.

S12). Pseudo colour (blue) has been used to represent the orange fluorescence due to the absence of the orange colour in the processing software of the microscope (Fig. S12). The merged fluorescence appears cyan (blue + green) and it clearly shows that most of the compound enters the organelle intact (Fig.S12-D). However, unlike NMR inside cell some dissociation was observed within 1h (as seen in the red channel image in Fig. S12-C). The dissociated daq was also found to co-localize with the mitotracker green further emphasizing that **2** entered in the organelle and started to dissociate over a period of time (Fig. S12-E).

Table 1. *In vitro* cytotoxicity (μM) data of **1** and **2** in normoxia and hypoxia [a]

		Normoxia [b]		Hypoxia [c]	
		1	**2**	**1**	**2**
MCF-7	-	85.61(4)	28.78(5)	79.29(1)	17.96(1)
	+ H_2A [d]	56.49(6)	16.40(3)	56.57(1)	17.25(1)
A549	-	109.8(1)	25.16(4)	93.99(2)	14.13(2)
	+ H_2A [d]	84.5(2)	21.01(3)	73.30(3)	12.46(1)
HepG2	-	68.59(5)	30.32(3)	73.51(1)	29.38(1)
	+H_2A [d]	53.72(4)	21.34(2)	58.42(1)	26.44(2)
HeLa*WT*	-	81.75(3)	21.64(2)	ND	ND
HFF-1	-	125.4(3)	28.39(3)	ND	ND

[a] Data reported are mean of at least two independent experiments. Standard deviation between individual data are reported in parenthesis. [b] at 21% O_2 concentration, [c] at 1.5 % O_2 concentration, [d] H_2A = ascorbic acid (500μM) Statistical significance (*p* value) of all data reported are of ≤ 0.05. ND = not determined.

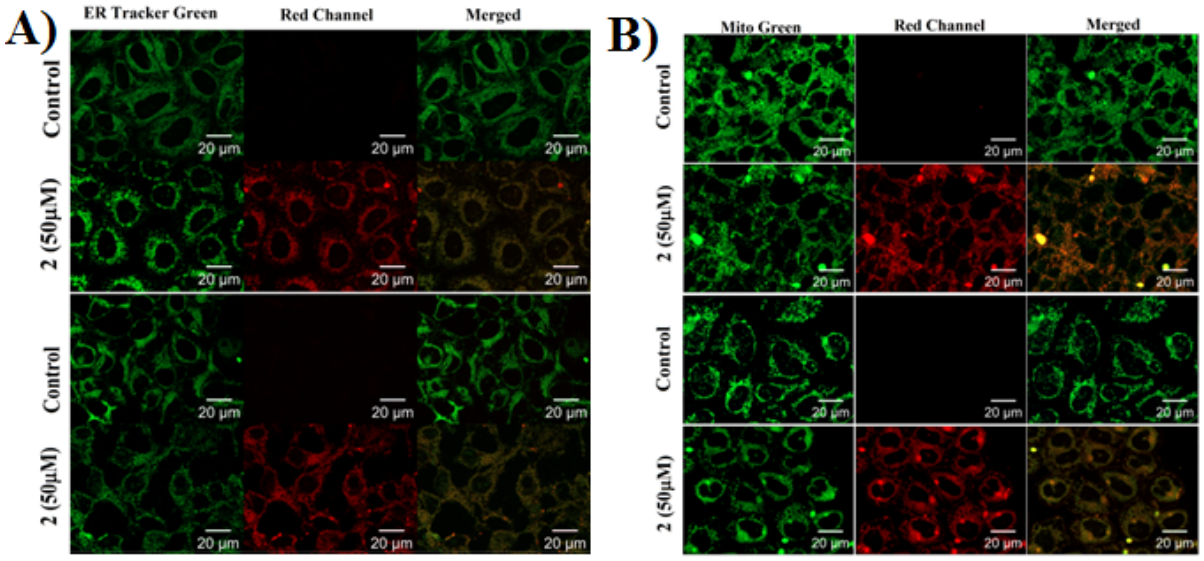

Fig. 4. Fluorescence images of (A) HeLa*WT* (above) and MCF-7 (below), treated with **2** (50μM) for 10 h. Green fluorescence of ER-Tracker Green™ shows endoplasmic reticulum and the red fluorescence originates from cells treated with **2**. Merged fluorescence images showed co-localisation of the dye and **2** in ER, (B) MCF-7 (above) and HeLa*WT* (below) treated with **2** (50μM) for 10 h. Green fluorescence of MitoTracker Green™ showed mitochondria and the red fluorescence originated from cells treated with **2**. The merged fluorescence image showed co-localisation of dye and **2** in mitochondria. All images captured at 63X magnification in Zeiss apotome microscope.

The apotome microscopy images of **2** treated cells taken after 10 h of incubation showed red fluorescence of the free daq present in the endoplasmic reticulum (ER, m = 0.55), mitochondria (m = 0.59) in HeLa*WT* (Fig. 4, Fig. S15-S17). The localization capability of **2** is due to the daq since the free daq also localised in ER, mitochondria and lysosome (Fig. S14). Co-localisation microscopy data of **2** with LysoTracker Green DND 26^{TM} in either MCF-7 or HeLa*WT* showed that there is almost no lysosome population (Fig. S17) which suggests that lysosomes were affected due to the treatment with **2**. On the other hand, free daq treated cells shows plenty amount of lysosome population with respect to control (Fig. S14). Probable reason of such observation lies behind the effect of cellular pH which here plays a role in stability and effectivity. Major activity of **2** against lysosomes by reduction of its population may be due to the acidic pH in lysozomes (pH ~ 4.5); leading ot its faster dissociation and thus formation of the active phosphoramide mustard. Hence, the localisation and action of **2** is cumulatively influenced by the phosphoramide group attached. In this connection, it was also found from the bright field images that treatment of **2** with both MCF-7 and HeLa*WT* produces vacuoles and budding on cell surface (Fig. S18) which are known consequences of cellular stress.[42]

3.5. Cell cycle, mitochondrial stress, ROS generation and apoptosis

The fluorescence imaging of the cells treated with **2** indirectly suggests that **2** mostly releases the daq and the active mustard inside the targeting organelles in cell. Similar to many nitrogen mustards [48, 49] the cell cycle progression was inhibited by **2** in G2/M phase. In contrast the more stable **1** arrested the cell cycle at S phase (Table S7 & Fig. 5A). Thus **1** inhibited the DNA replication process whereas **2** inhibited the cell cycle at the mitosis stage. We checked the effect of **1** and **2** on nuclear morphological changes using DAPI. Microscopic images showed that treatment with **1** produced dense nuclei and that with **2** rendered swelled/enlarged nuclei (Fig. S19). Elongated nuclei being an indication of late stage of cell division this data correlated with G2/M phase arrest by **2** in MCF-7. The analysis of the genomic DNA from cells treated with either **1** or **2**, showed ladder like pattern of degraded DNA oligonucleosomal fragment with approximate steps of roughly 180-185bp which is indicative of induction of apoptosis (Fig. 5C).[50]

We studied the involvement of ROS by 2′,7′-dichlorofluorescin diacetate (DCFH-DA) assay. It was found that there is significant enhancement of ROS population when MCF-7 cells were treated with **1** or **2** (Fig. S20). The effect of ROS accumulation has to be indirect since it is observed for both **1** and **2** and although **2** has a quinone motif but **1** has no such motif which may be directly involved in ROS generation. **2** significantly altered the mitochondrial transmembrane potential ($\Delta\Psi_m$) indicating that it may favor the intrinsic pathway of apoptosis (Fig. 5B). Apart from the above **1** and **2** also activated caspase 7 and 8 (Fig. 5D-E). It was found that there was more activation of caspase 8 by **2** signifying that the apoptosis in case of **2** may have relatively more contribution from extrinsic pathway compared to **1**.

The results discussed above suggests that apart from targeting the nucleus by the active mustard motif **2** also targets the ER, mitochondria and lysosome. The interaction of the daq with biomolecules inside cell may further promote the hydrolysis of **2** to form the free phosphoramic mustard and daq. The free phosphoramic mustard then released the alkylating $-HN(CH_2CH_2Cl)_2$ moiety. The interaction of the anthraquinone and the $-HN(CH_2CH_2Cl)_2$ moiety of **2**, with biomolecules in endoplasmic reticulum, including proteins and the RNA may induce ER stress. All the above activity inside the ER and the mitochondria may lead to disruption of cellular growth and promote apoptosis.

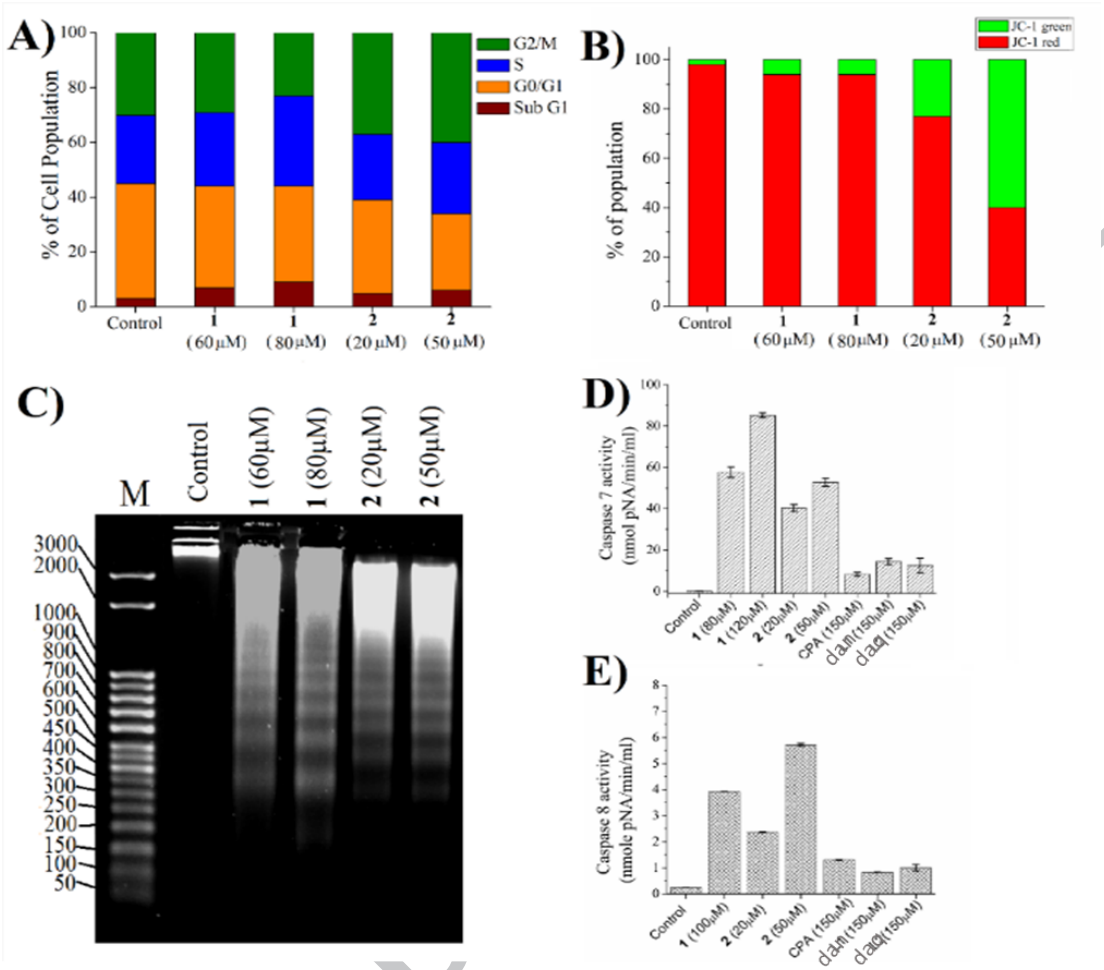

Fig. 5. Pathways of cellular toxicity of **1** and **2** probed against MCF-7. Cells were treated with different concentrations of compounds for 24 h of incubation period. Typical bar diagram showing: A) cell cycle analysis and B) population of cells undergoing change in mitochondrial membrane potential upon treatment with different concentration of compounds; C) Agarose gel electrophoresis image showing DNA extracted from MCF-7 after treatment. Isolated DNA from treated cells showed fragmented DNA formed in ladder like pattern Fragmented bands are of multiplier of 180bp. M stands for known base pair (50 bp) marker step ladder for fragment identification.; Activation profile of D) Caspase7 and E) Caspase 8 activation upon treatment with compounds and their precursors (for comparison). In all cases control lane represents DMSO (vehicle) in treatment Error bar in diagram represent standard deviations in data.

3.6. Inhibition of cell migration activity

Compound **1** and **2** interferes with the ability of the cancer cells to migrate (metastasis) hence interfering with the spread of cancer. Cell migration inhibitory activity of **1** (8 & 15 µM) and **2** (3 & 6 µM) were evaluated by means of wound healing assay (scratch assay) against MCF-7 using IC_{10} dose. Non-healing of artificial wound on monolayer of cells was observed during 48 h of treatment (Fig. S21A-B). In addition, the cells did not proliferate even after removal of the compounds and although the cells were replenished in fresh growth medium for further 48 h (Fig. S21C). The above results suggest that the compounds exhibit strong anti-migratory activity. The wound area was rather increased over time due to detachment of cells, as an effect of **1** or **2** (Fig. S21C).[51]

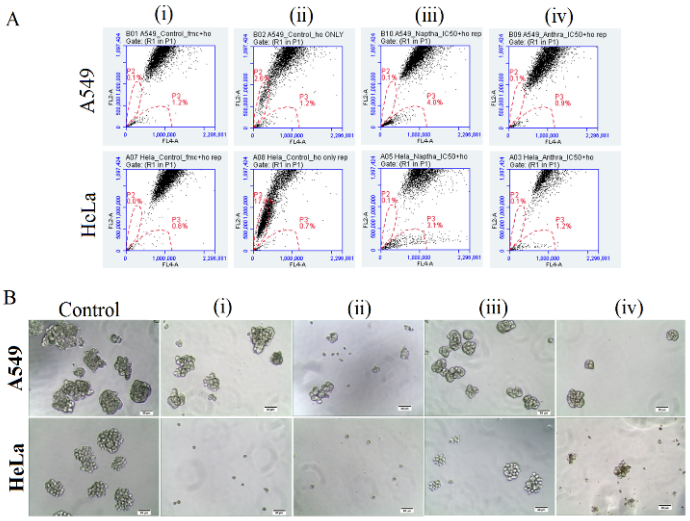

Fig. 6. Effect of **1** & **2** against cancer stem cells. A) Side population analysis of A549 and HeLa*WT* treated with **1**-**2** for 48 h.; (i) with inhibitor (FMC), (ii) control, (iii)**1** (IC_{50}), (iv) **2** (IC_{50}); Gate indicative of SP cells in experiments and B) Bright field images of spheroids after treatment of **1**-**2** at different concentration against A549 and HeLa*WT* for 5th day. Images captured at 10X magnification. (i) **1** (IC_{10}), (ii) **1** (IC_{50}), (iii) **2** (IC_{10}), (iv) **2** (IC_{50}).

3.7. Inhibition of cancer stem cell (CSC) population

Flow cytometry studies can be employed to study side population (SP) which is a sub-population of cells with distinct characteristics of cancer stem cells (CSC).[52, 53] The Hoechst 33342 dye exclusion method was used to select this population. We found that there is a significant decrease in SP-cells in both A549 and HeLa*WT*, when treated with IC_{50} dose of **1** and **2** for 48 h (Fig. 6A and Table S8). Encouraged by this result we probed the CSC-spheroid disruption ability of **1** and **2** *in vitro*.

It is quite well known that cancer stem cells have the property of self-renewal due to their stem / progenitor activity, demonstrated as sphere-formation ability.[20] Cells were treated with compounds at IC_{10} concentrations (A549 IC_{10} of **1** = 35 µM, **2** = 15 µm; HeLa*WT* IC_{10} of **1** = 40 µM, **2** = 5 µM) along with their IC_{50} dose. Cells were treated with respective IC_{50} and IC_{10} doses on the first day. Progressive evaluation until the 5th day showed that both the compounds significantly inhibited sphere formation.

However, the more stable **1** proved to be most effective in disruption of CSC spheres as compared to **2** at IC_{10} dose (Fig. 6B). It suggests that **1** is more potent than **2** in inhibiting sphere-formation. **1** almost completely impeded sphere-formation ability of CSCs at both IC_{10} and IC_{50} doses, but, IC_{10} dose of **2** could only inhibited approximately 1/3rd of sphere-forming ability with respect to the control (Table S8).

4. Conclusions

The two phosphoramide mustards are stable in solution for at least 10 h. Compound **2** showed enhanced reactivity when D_2O was substituted for H_2O unlike **1** which is stable for 48 h. The above reactivity trend suggested that the presence of suitable nucleophile would enhance the reactivity and indeed the presence of hydroxide anion enhanced its reactivity as seen in phosphorous NMR data. Confocal microscopy of **2** suggested intact accumulation of **2** in cellular organelles viz. mitochondria. It also accumulated in multiple cellular organelles and impaired their function. The degradation of lysosome by **2** was visible from the decrease of the lysosomal population on treatment. Treatment with **1** and **2** also led to enhancement of

ROS accumulation in the cells (Scheme 3). The dissociation of **2** inside cells over time released the active phosphoramide mustard which helped induce alkylation leading to higher toxicity, proposed in scheme 3.

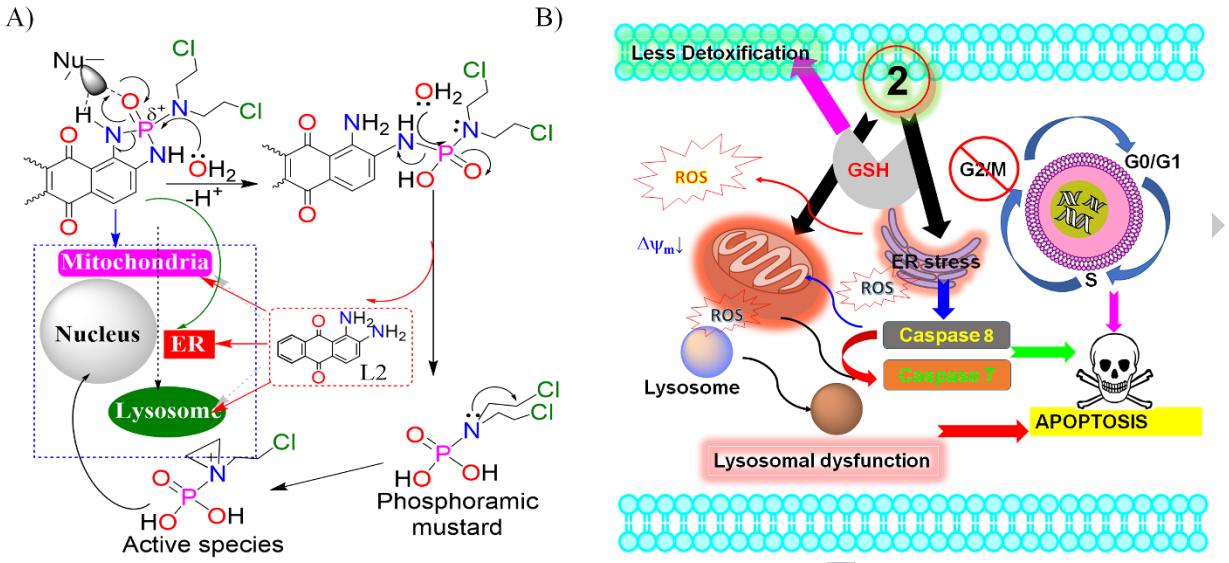

Scheme. 3. A) Plausible activation pathways of **2** by elimination of daq and active mustard group; B) mechanism of action of **2** *in vitro*.

Although **1** requires higher dosage to kill cancer cells, it should also be noted that it is less toxic to normal cells. Even at sub-toxic concentrations these compounds demonstrated good activity against cell migration and self-renewal growth of CSCs which is highly encouraging. **1** and **2** showed cell cycle arrest in S- and G2/M phase respectively leading to apoptosis. The inhibition of self-renewal of CSCs suggested that these phosphoramides are potential candidates in reducing the scope of relapse of cancer. In future, we should be able to improve upon the stability, therapeutic activity and generate improved phosphoramide mustards using the insight gained from these results.

Statistical analysis

Data are presented as statistical means with SD (Standard deviations). The cut-off *p* value for significance was set at *p*, 0.05. and considered statistically significant. The statistical comparison analysis was done using the one sample t- test. Graphpad Prism® V5.04 was used to perform all statistical analysis.

Acknowledgments

We sincerely acknowledge SERB- India for financial support (vide project no. SB/S1/IC-02/2014 and EMR/2017/002324). S.S. acknowledges the grant support provided by the Wellcome trust-DBT India Alliance (IA/I/13/1/500908). We are also thankful to IISER Kolkata and National Institute of Biomedical Genomics for infrastructural support. We extend our sincere thanks to Dr. Rupak Dutta, Dr. Bidisha Sinha for useful suggestions and help. S.B. is thankful to CSIR-India, S.A. is thankful to UGC, K.V. is thankful to DST-INSPIRE for research fellowship and S.K.D. to DST-India (vide project no. SB/S1/IC-02/2014) for providing post-doctoral research fellowship. We sincerely acknowledge the help by Mr. Santanu Das and Mr. Saptarshi Maji from Dr. Arnab Gupta's laboratory for the live cell confocal microscopy.

Appendix A. Supplementary data

CCDC 1487144 contains the supplementary crystallographic data for **1**. Data can be obtained free of charge via http://www.ccdc.cam.ac.uk/conts/retrieving.html, or from the Cambridge Crystallographic

Data Centre, 12 Union Road, Cambridge CB2 1EZ, UK; fax: (+44) 1223-336-033; or e-mail: deposit@ccdc.cam.ac.uk.

Supplementary data to this article can be found online at https://doi.org/10.1016/.....

References

[1] D.J. Huggins, W. Sherman, B. Tidor, J. Med. Chem., 55 (2012) 1424-1444.
[2] J.M. Tucker, C. Davis, M.E. Kitchens, M.A. Bunni, D.G. Priest, H.T. Spencer, F.G. Berger, Cancer Lett., 187 (2002) 153-162.
[3] P.-Y. Yang, K. Liu, M.H. Ngai, M.J. Lear, M.R. Wenk, S.Q. Yao, J. Am. Chem. Soc., 132 (2010) 656-666.
[4] H. Mayumi, M. Umesue, K. Nomoto, Immunobiology, 195 (1996) 129-139.
[5] M.B. Haselberger, T.L. Schwinghammer, Ann. Pharmacother., 29 (1995) 918-921.
[6] N.E. Sladek, R. Kollander, L. Sreerama, D.T. Kiang, Cancer Chemother. Pharmacol., 49 (2002) 309-321.
[7] B.J.S. Sanderson, A.J. Shield, Mutat. Res., Fundam. Mol. Mech. Mutagen., 355 (1996) 41-57.
[8] A.R. Watson, C.P. Rance, J. Bain, Br Med J (Clin Res Ed), 291 (1985) 1457-1460.
[9] D.T. Boumpas, H.A. Austin, 3rd, E.M. Vaughan, C.H. Yarboro, J.H. Klippel, J.E. Balow, Ann Intern Med, 119 (1993) 366-369.
[10] T.J. Stillwell, R.C. Benson, Jr., Cancer, 61 (1988) 451-457.
[11] P.J. Cox, Biochem. Pharmacol., 28 (1979) 2045-2049.
[12] W. Matsui, C.A. Huff, Q. Wang, M.T. Malehorn, J. Barber, Y. Tanhehco, B.D. Smith, C.I. Civin, R.J. Jones, Blood, 103 (2004) 2332-2336.
[13] D.J. Pearce, D. Taussig, C. Simpson, K. Allen, A.Z. Rohatiner, T.A. Lister, D. Bonnet, Stem Cells, 23 (2005) 752-760.
[14] I. Ma, A.L. Allan, Stem Cell Rev. Rep., 7 (2011) 292-306.
[15] J. Marx, Science, 317 (2007) 1029-1031.
[16] L.V. Nguyen, R. Vanner, P. Dirks, C.J. Eaves, Nat. Rev. Cancer, 12 (2012) 133-143.
[17] M. Dean, T. Fojo, S. Bates, Nat. Rev. Cancer, 5 (2005) 275-284.
[18] J.E. Visvader, G.J. Lindeman, Nat. Rev. Cancer, 8 (2008) 755-768.
[19] J.E. Visvader, G.J. Lindeman, Cell Stem Cell, 10 (2012) 717-728.
[20] T. Reya, S.J. Morrison, M.F. Clarke, I.L. Weissman, Nature, 414 (2001) 105-111.
[21] J. Kaiser, Science, 347 (2015) 226-229.
[22] S. Sell, Crit Rev Oncol Hematol, 51 (2004) 1-28.
[23] K. Laws, G. Bineva-Todd, A. Eskandari, C. Lu, N. O'Reilly, K. Suntharalingam, Angew. Chem., Int. Ed., 57 (2018) 287-291.
[24] K. Suntharalingam, W. Lin, T.C. Johnstone, P.M. Bruno, Y.-R. Zheng, M.T. Hemann, S.J. Lippard, J. Am. Chem. Soc., 136 (2014) 14413-14416.
[25] S. Palomeras, S. Ruiz-Martinez, T. Puig, Molecules, 23 (2018) 2193/2191-2193/2116.
[26] M. Venugopal, C.D. Reddy, M. Bavaji, Indian J. Chem., Sect. B Org. Chem. Incl. Med. Chem., 40B (2001) 822-827.
[27] H. Zimmer, A.D. Sill, Arzneimittel. Forsch., 5 (1964) 150-151.
[28] H. Doepp, D. Doepp, Sci. Synth., 17 (2004) 223-355.
[29] W.L.F. Armarego, D.D. Perrin, Purification of Laboratory Chemicals, Fourth Edition, 1997.
[30] O.M. Friedman, A.M. Seligman, J. Am. Chem. Soc., 76 (1954) 655-658.
[31] M.A. Goodell, K. Brose, G. Paradis, A.S. Conner, R.C. Mulligan, J. Exp. Med., 183 (1996) 1797-1806.
[32] S. Singh, N. Bora-Singhal, J. Kroeger, H. Laklai, P. Chellappan Srikumar, PLoS One, 8 (2013) e55982.
[33] S. Singh, J. Trevino, N. Bora-Singhal, D. Coppola, E. Haura, S. Altiok, S.P. Chellappan, Mol. Cancer, 11 (2012) 73.
[34] G. Dontu, W.M. Abdallah, J.M. Foley, K.W. Jackson, M.F. Clarke, M.J. Kawamura, M.S. Wicha, Genes Dev., 17 (2003) 1253-1270.

[35] Z. Fei, I. Neda, H. Thonnessen, P.G. Jones, R. Schmutzler, Phosphorus, Sulfur Silicon Relat. Elem., 131 (1997) 1-23.
[36] R. Sonnenburg, I. Neda, H. Thonnessen, P.G. Jones, R. Schmutzler, Z. Anorg. Allg. Chem., 626 (2000) 412-420.
[37] M. Farkens, I. Neda, A. Fischer, P.G. Jones, R. Schmutzler, Z. Naturforsch., B Chem. Sci., 48 (1993) 853-859.
[38] F. Galindo, N. Kabir, J. Gavrilovic, D.A. Russell, Photochem. Photobiol. Sci., 7 (2008) 126-130.
[39] M.J. Marín, P. Thomas, V. Fabregat, S.V. Luis, D.A. Russell, F. Galindo, ChemBioChem, 12 (2011) 2471-2477.
[40] O. Swiech, A. Mieczkowska, K. Chmurski, R. Bilewicz, J. Phys. Chem. B, 116 (2012) 1765-1771.
[41] K.N. Prasad, C. Hernandez, J. Edwards-Prasad, J. Nelson, T. Borus, W.A. Robinson, Nutr. Cancer, 22 (1994) 233-245.
[42] C.M. Kurbacher, U. Wagner, B. Kolster, P.E. Andreotti, D. Krebs, H.W. Bruckner, Cancer Lett., 103 (1996) 183-189.
[43] P.D. Josephy, B. Palcic, L.D. Skarsgard, Nature, 271 (1978) 370-372.
[44] S. Ohno, Y. Ohno, N. Suzuki, G.-I. Soma, M. Inoue, Anticancer Res., 29 (2009) 809-815.
[45] S.B. Prasad, G. Rosangkima, B.M. Nicol, Eur. J. Pharmacol., 645 (2010) 47-54.
[46] J.C. Vera, C.I. Rivas, F.V. Velasquez, R.H. Zhang, I.I. Concha, D.W. Golde, J. Biol. Chem., 270 (1995) 23706-23712.
[47] J.C. Vera, C.I. Rivas, J. Fischbarg, D.W. Golde, Nature, 364 (1993) 79-82.
[48] P.M. O'Connor, D.K. Ferris, M. Pagano, G. Draetta, J. Pines, T. Hunter, D.L. Longo, K.W. Kohn, J. Biol. Chem., 268 (1993) 8298-8308.
[49] S. Inturi, N. Tewari-Singh, C. Agarwal, C.W. White, R. Agarwal, Mutat. Res., Fundam. Mol. Mech. Mutagen., 763-764 (2014) 53-63.
[50] A.H. Wyllie, Nature, 284 (1980) 555-556.
[51] C.-C. Liang, A.Y. Park, J.-L. Guan, Nat. Protocols, 2 (2007) 329-333.
[52] A. Challen Grant, H. Little Melissa, Stem Cells, 24 (2006) 3-12.
[53] A. Golebiewska, N.H.C. Brons, R. Bjerkvig, S.P. Niclou, Cell Stem Cell, 8 (2011) 136-147.

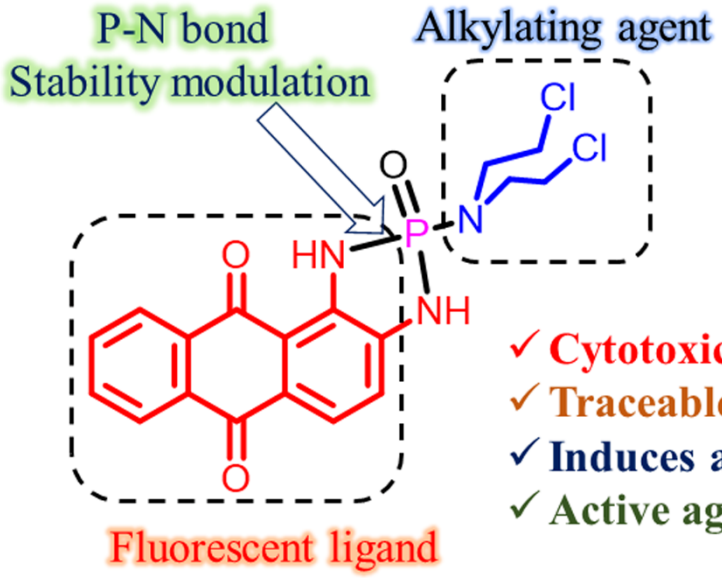

- ✓ Cytotoxic
- ✓ Traceable
- ✓ Induces apoptosis
- ✓ Active against Cancer stem cells